Liquid hydrogen tank chill and no-vent fill prediction using computational fluid dynamics

Justin M Pesich[1], Daniel M Hauser[1], Kiyotaka G Yamashita[2], Michael C Baker[2] and Barbara A Sakowski[1]

[1] NASA Glenn Research Center, 21000 Brookpark Rd, Cleveland, Ohio, 44135, USA
[2] HX5, LLC., 3000 Aerospace Parkway, Brook Park, Ohio, 44142, USA

Email: justin.m.pesich@nasa.gov

Abstract. Cryogenic tank chill and fill is an important cryogenic fluid management technology that supports and enables many of NASA's long-duration space missions. For no-vent fill, the receiver tank pressure remains below the supply tank pressure during the entire duration of the fill so that the tank does not require venting. This is especially advantageous for tank fill operations in low gravity where the position of the liquid is not always known and venting the tank may cause loss of propellant by venting liquid. In lieu of expensive tests conducted on-orbit, accurate computational models capable of predicting receiver tank pressure during cryogenic propellant tank fill may be used to reduce system and propellant mass as well as mission risk. However, these numerical models must be validated or anchored to test data. This study presents computational fluid dynamics (CFD) models with conjugate heat transfer that are used to predict a liquid hydrogen tank chill and no-vent fill ground test conducted at Lewis Research Center (now Glenn Research Center) in 1991. The specific test case chosen for model validation implemented an upward-facing jet near the bottom of a cylindrical 34-liter tank. CFD predictions are compared to experimental measurements of tank pressure, fill level, and wall temperature. The CFD results show reasonable agreement to the test data but overpredict the pressure collapse near the end of the fill despite the liquid jet penetrating the liquid-vapor interface.

1. Introduction

Cryogenic tank chill and fill is an important cryogenic fluid management technology that supports and enables many of NASA's long-duration space missions. For no-vent fill, the pressure of the receiver tank remains below the maximum expected operating pressure during the entire duration of the fill so that the tank does not require venting. This is especially advantageous for tank fill operations in low gravity where the position of the liquid is not always known and venting the tank may cause loss of propellant by venting liquid. Therefore, accurate computational models capable of predicting receiver tank pressure during cryogenic propellant tank fill would reduce system and propellant mass as well as mission risk.

The objective of this study is to perform model validation of a liquid hydrogen (LH2) tank chill and no-vent fill using an upward facing pipe under normal gravity (1-g) using three different commercial computational fluid dynamics (CFD) codes: Siemens Simcenter STAR-CCM+, ANSYS Fluent, and

Flow Science Flow3D. The hydrogen no-vent fill testing in a 1.2 cubic foot (34 liter) tank data is used for model validation [1-2].

In this paper, an overview of the test setup is provided. Next, the computational model setup including the mesh, initial conditions, and boundary conditions are provided. Finally, the CFD model results are compared to the experiment. Time histories of tank pressure, fill level, wall temperature, interfacial mass transfer rate, and phase distribution are analyzed. Last, the presence of helium in the tank was investigated using a lower-fidelity nodal SINDA/Fluint model.

2. Experimental Overview

The liquid hydrogen no-vent fill ground test results are reported by Moran et al. [1] and more generally reported as part of a larger test campaign in Moran et al. [2]. The tests reported in [1] are for LH2 no-vent fill testing with a 1.2 cubic foot receiver tank using three different liquid injection methods: top spray, upward pipe discharge, and bottom diffuser. Test Number 9093G was chosen for CFD model validation which incorporated the upward pipe discharge injection method.

The tank has an internal height of 20 inches, inside diameter of 12.5 inches, and two domes on each end of the cylindrical yielding an internal volume of 1.2 cubic feet. The tank wall thickness is 0.03 inches. No details of the injector pipe or tank lid were provided or found in NASA databases (no drawings or schematics). This includes the injector pipe diameter and axial height of the pipe exit. Details of the entire lid assembly are completely unknown. The lack of geometric definition is a significant source of uncertainty for performing model validation. The inlet pipe diameter was assumed to be 0.75 inches and the outlet was assumed to be 4.7 inches from the bottom of the tank based on engineering judgement.

For each fill test, some experimental quantities were only reported as averaged values and are listed in table 1 for Test Number 9093G. A single value for the initial temperature was reported; however, from the time-dependent fluid and wall temperature sensor data, a more accurate initial temperature distribution was attained. Unfortunately, no time-dependent mass flow rate or inlet temperature was reported. Based on the inlet temperature (P_{sat}(18.55K) = 8.2 psia) and initial tank pressure ($P_{initial}$ = 3.8 psia), it is expected that the liquid flashed as it entered the receiver tank. This suggests there is uncertainty on the measured mass flow rate and inlet temperature, and that constant values are not representative of what occurred for the entire fill duration.

It is noted here that gaseous helium was used to purge the receiver tank between tests, so trace amounts of helium may have become trapped in the tank. This is another source of uncertainty in the experiment and would have implications on the experimental tank pressure and affect the validation comparison.

Table 1. Averaged measured test quantities for test number 9093G

Fill Configuration	Inlet Temperature	Inlet Flow Rate	Initial Tank Pressure	Final Fill Level
	K	kg/s	psia	% by volume
Upward pipe	18.55	0.034	3.8	96

3. Computational Model

3.1. Geometry and Mesh

Computational models were built separately in STAR-CCM+, Fluent, and Flow3D. Each model used the same full three-dimensional input geometry and constructed very similar meshes shown in figure 1 (meshes are shown on a two-dimensional slice). All three models included the solid wall to solve for the conjugate heat transfer. Each code used a cell size of 4.0 mm for the bulk mesh and implemented various refinement techniques at the wall beneficial to each code. The Fluent mesh employed adaptive mesh

refinement (AMR) to speed-up simulation and more accurately resolve the liquid jet, highlighted in figure 1.

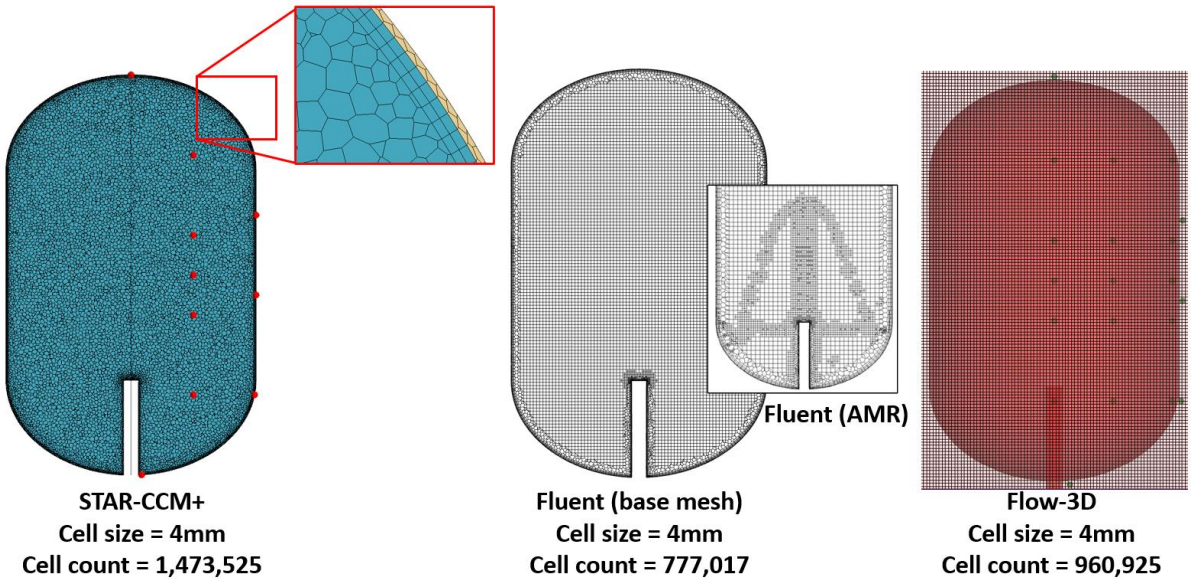

Figure 1. Mesh details for each commercial CFD code

3.2. Initial Conditions and Boundary Conditions

The initial conditions and boundary conditions are provided in figure 2. The initial tank pressure was set to the initial pressure measured in the experiment of 3.8 psia. The initial temperature distribution was determined by the initial experimental wall temperatures and was linearly interpolated between each value at 0, 4, 9, 13, and 20 inches along the tank height.

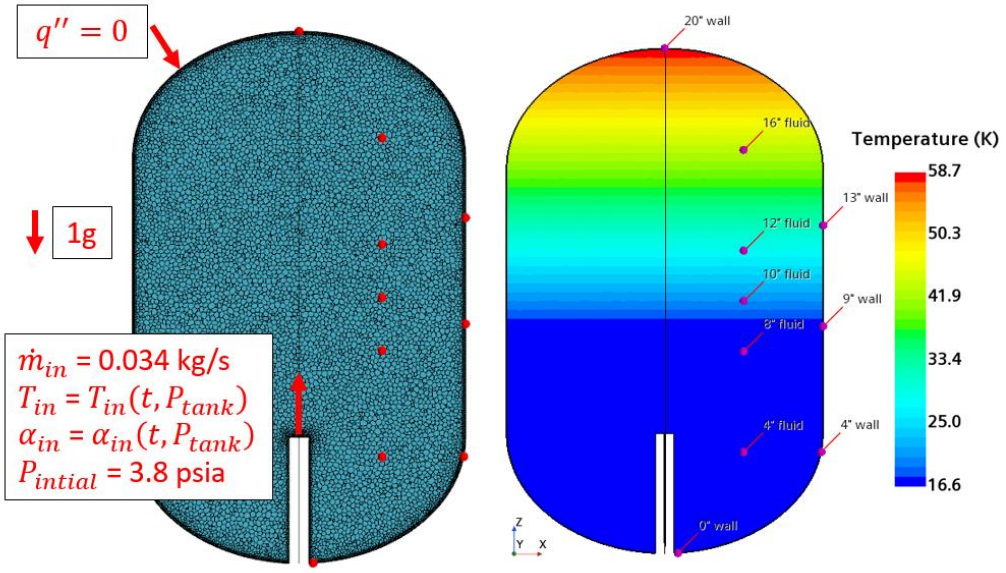

Figure 2. Boundary conditions and initial conditions

The external solid wall boundaries were assumed to be adiabatic because the heat leak is unknown. The inlet mass flow rate was assumed to be constant at 0.034 kg/s for the entire duration of the fill. As

described earlier, the liquid flashed as it entered the tank since the initial pressure was below the saturation pressure at the inlet temperature. Therefore, the inlet void fraction and temperature were implemented as time-dependent variables until the simulated tank pressure reached the saturation pressure at the inlet temperature. The time-dependent inlet temperature is given by equation (1). If the simulated tank pressure is below the saturation pressure at the experimental inlet temperature, the inlet temperature is set to the saturation temperature of the current tank pressure. The saturation temperature in the CFD model was defined by the Clausius-Clapeyron relation given by equation (2).

The time-dependent void fraction was calculated by conservation of enthalpy for liquid flashing across an orifice. The quality at the exit of the jet is given by equation (3), thus the void fraction can be computed by equation (4). These expressions are evaluated using the tank pressure computed by the CFD model. Note that the slip ratio, *S*, was assumed to be unity as in most models. Once the simulated tank pressure reached the saturation pressure at the inlet temperature, the void fraction was set to zero.

$$\begin{aligned} &if\ P_{tank} < P_{sat}\left(T_{inlet,exp}\right)\ then\ T_{inlet} = T_{sat}(P_{tank}) \\ &if\ P_{tank} \geq P_{sat}\left(T_{inlet,exp}\right)\ then\ T_{inlet} = T_{inlet,exp} \end{aligned} \tag{1}$$

$$P_{sat}(T_{cell}) = P_{ref} exp\left[\frac{H_{vap}}{R}\left(\frac{1}{T_{ref}} - \frac{1}{T_{cell}}\right)\right] \tag{2}$$

$$X = \frac{Cp_{liq}[T_{inlet} - T_{sat}(P_{tank})]}{H_{vap}} \tag{3}$$

$$\alpha_{vap} = \left[1 + \frac{1-X}{X}\frac{\rho_{vap}}{\rho_{liq}}S\right]^{-1} \tag{4}$$

3.3. Material Properties

The tank structure material is modeled as stainless steel 304 with temperature-dependent material properties. The liquid phase was assumed incompressible, and the vapor phase was assumed to be a compressible ideal gas. Both phases used constant properties at the experimental inlet temperature. All material properties were taken from NIST Refprop.

3.4. Physics Models

The CFD model considered the full three-dimensional geometry under normal gravity (1-g). The Volume of Fluid multiphase solver was used to model the two-phase flow. Since the Reynolds number based on jet diameter is 1.4e5, the flow was considered turbulent. The numerical discretization schemes for the flow equations, turbulence, and energy were second order.

Interfacial mass transfer was modeled using the Schrage relation defined in equation (5) with units of kg/m^{2}s [3]. This model accounts for the condensation and evaporation mass transfer at liquid-vapor interface and is dependent on the accommodation coefficient, σ, which was set to 0.001 for all three codes. The saturation pressure at the temperature of the cell is defined by the Clausius-Clapeyron relation previously defined in equation (2).

$$\dot{m}_i = \left(\frac{2\sigma}{2-\sigma}\right)\left[\frac{M}{2\pi R T_{cell}}\right]^{1/2}\left(P_{sat}(T_{cell}) - P_{abs}\right) \tag{5}$$

4. Results and Discussion

4.1. Fill Level

The STAR-CCM+ fill level prediction is compared to the experiment in figure 3. Oscillations in the experimental fill level are observed during the middle section of the test. The upward liquid jet acted as a forced perturbation that excited the liquid-vapor interface inducing a slosh mode for that range of fill level. The oscillations are visible in the experimental data because the fill level was measured using a capacitance type probe with discrete point sensors. As the liquid sloshed, the fill level seemingly rose and fell due to the off-center discrete point sensors. Contrary, the CFD fill level computed by dividing the current liquid volume by the tank volume resulting in a linear response due to the constant flow rate.

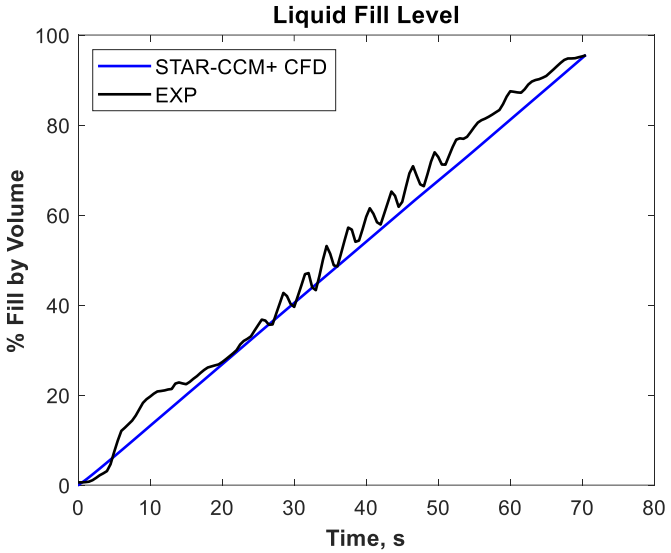

Figure 3. Comparison of liquid fill level between CFD and experiment

The oscillations are observed the STAR-CCM+ CFD prediction highlighted in figure 4 by the phase distribution contour plots. The oscillations in the experimental fill level begin around 25 seconds and finish around 55 seconds. The STAR-CCM+ CFD results show an angled interface beginning at 25 seconds, which becomes more severe at 35 and 45 seconds. A flat interface is observed at 55 seconds indicating the sloshing has damped out.

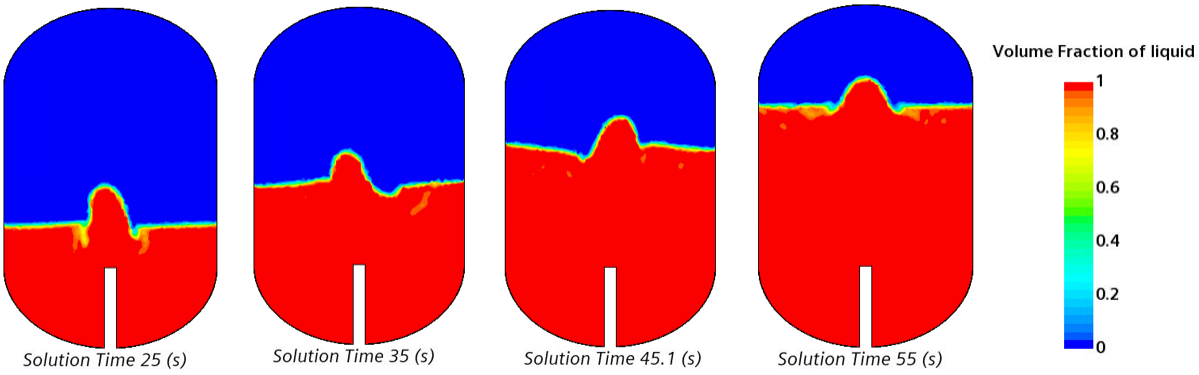

Figure 4. STAR-CCM+ CFD fill level evolution highlighting induced slosh mode

4.2. Tank Pressure and Interfacial Mass Transfer

The tank pressure prediction for all three CFD codes is compared to the experiment in figure 5. The pressure response can be split into three sections denoted on the plot: 1) flashing of inlet liquid;

chilldown of tank wall, 2) ullage vapor condensation on liquid-vapor interface; continued vaporization, and 3) ullage compression. Both the Fluent and Flow3D predict the initial pressure rise well during section 1, whereas STAR-CCM+ computes a slower pressure rise. All three codes show similar pressure responses during section 2 and 3. Notably, all three codes fail to predict the ullage compression in section 3, which is clearly observed in the experimental pressure. This is attributed to an over-prediction in the condensation yielding flat pressure curves, despite all three codes predicting the liquid jet to penetrate the liquid-vapor interface which would significantly enhance condensation (highlighted in figure 4).

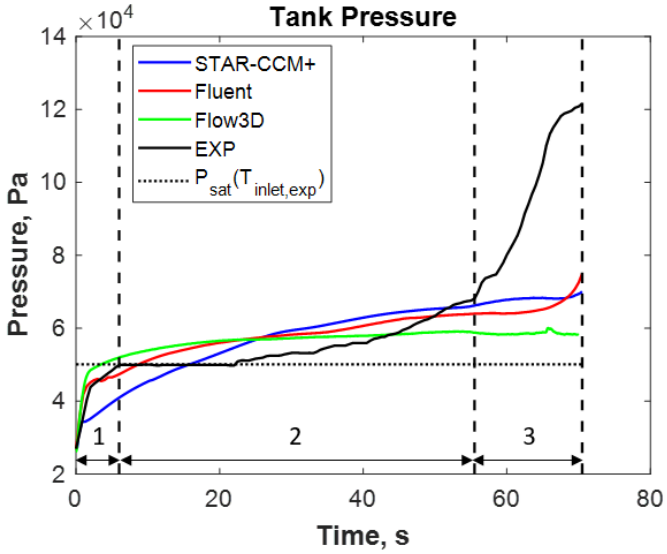

Figure 5. Comparison of tank pressure between CFD and experiment

The interfacial mass transfer rates for all three CFD codes are given in figure 6. The positive values are evaporation shown in figure 6(a), and the negative values are condensation shown in figure 6(b). STAR-CCM+ predicts a lower initial pressure rise in section 1 due to the lower evaporation rate seen in figure 6(a). The Flow3D evaporation rate displays the fastest rise while Fluent yields the largest evaporation rate; both attribute to the higher initial pressure rise, whereas STAR-CCM+ predicts a slower pressure rise. All three CFD codes predict similar condensation rates.

Differences in the evaporation rate can be explained by investigating the phase distribution for each code demonstrated in figure 7. STAR-CCM+ uses the High-Resolution Interface Capturing scheme, whereas Fluent and Flow3D implement a Geometric Reconstruction scheme. Note that although the Flow3D phase distribution is not shown, Flow 3D and Fluent phase distributions are very similar. STAR-CCM+ predicts a “misty” column of fluid while Fluent and Flow3D predict globs of liquid yielding a larger liquid surface area for evaporation to occur. This directly relates to a larger evaporation rate early in the fill process.

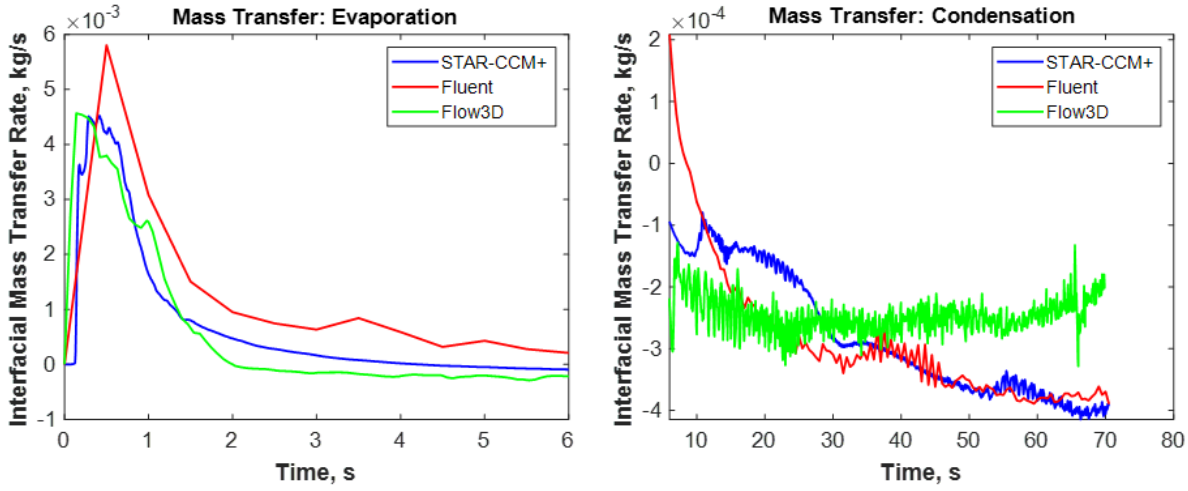

Figure 6. Interfacial mass transfer rates: evaporation (a) and condensation (b)

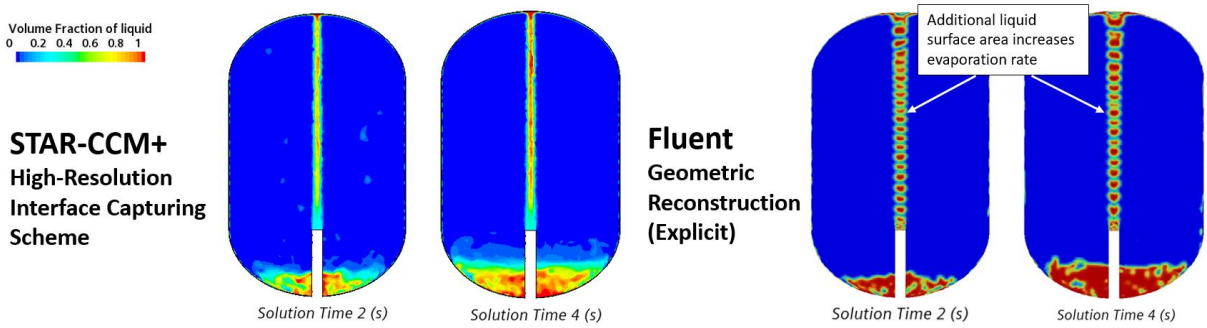

Figure 7. Comparison of phase distribution between STAR-CCM+ and Fluent

4.3. Presence of Helium and Wall Temperature

None of the CFD codes accurately captured the ullage compression at the end of the fill. As stated previously, it is possible that trace amounts of helium (a non-condensable gas) could have been trapped in the receiver tank during the purge process between tests. The effect of the presence of helium on the pressure response was studied using a SINDA/Fluint nodal model. In this model, the mass fraction of helium was set to 1.5% initially distributed in the bottom ullage nodes, and a heat load of 6 Watts was applied to the top dome of the tank. The computational model tank pressures are compared to the experiment in figure 8(a) and top wall temperature results are compared to the experiment in figure 8(b). The nodal model considered a case with and without helium and are both included in figure 8. From figure 8(a), the case without helium compares well to the CFD pressure results; however, the case with helium captures the ullage compression unlike any of the CFD predictions. Therefore, it is very possible there were trace amounts of helium trapped in the tank prior to the test. The presence of the non-condensable mitigates condensation which would increase the tank pressure especially at high fill levels.

Despite the differences in phase distribution early in the fill, Fluent and STAR-CCM+ both predict the initial chilldown of the tank with reasonable agreement to the experiment. Flow3D does not capture the entire chilldown to the inlet temperature. Flow3D's pressure prediction exceeds $P_{sat}(T_{inlet,exp})$ very quickly, so the liquid jet did not impinge on the top dome as long as Fluent and STAR-CCM+. Around 25 seconds, the experimental temperature abruptly increases and is assumed to be due to heat leak. All CFD models used an adiabatic boundary condition on the outer wall; however, the SINDA/Fluint model included a heat leak on the top dome where the top wall sensor is mounted. Both cases with and without helium predict the abrupt temperature rise, but only the case with helium captures the entire temperature

rise late in the fill. Not only did the helium cause the late pressure rise, but it also affects the temperature at the top of the tank.

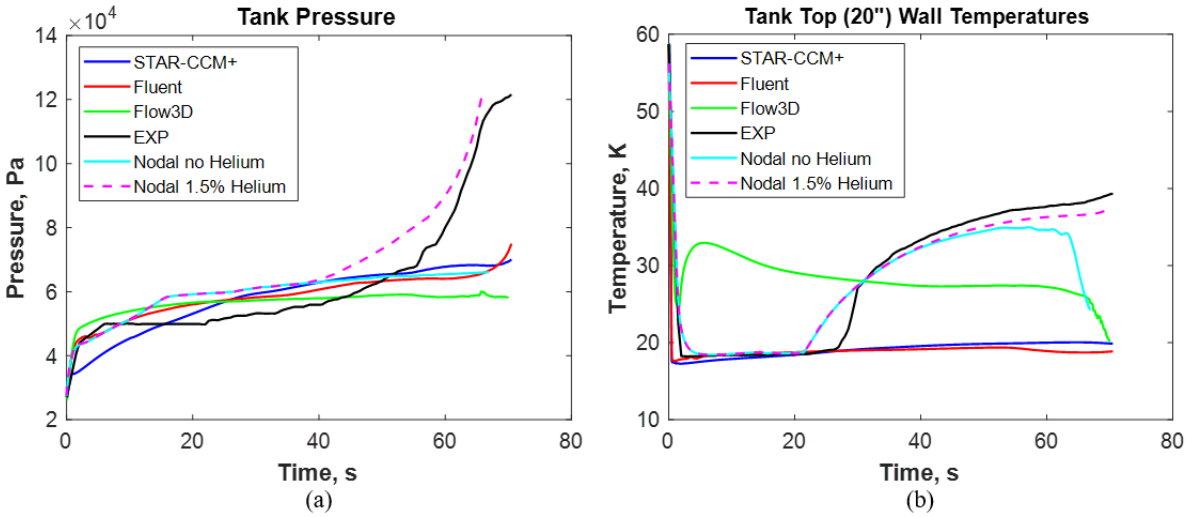

Figure 8. Comparison of pressure and top wall temperature between CFD, nodal, and experiment

5. Conclusions

A CFD validation study was carried out by modeling a liquid hydrogen no-vent fill experiment. Three commercial CFD codes were considered, namely STAR-CCM+, Fluent, and Flow3D. All three codes showed that the induced slosh mode due to the upward liquid jet perturbation was captured and compared well to the experiment. Fluent and Flow3D predicted the initial pressure rise reasonably well, while STAR-CCM+ predicted a slower pressure rise and a lower evaporation rate due to differences in the interface capturing scheme. None of the CFD codes accurately captured the ullage compression at the end of the fill. Further investigation using a SINDA/Fluint nodal model revealed the presence of helium affects the late pressure and temperature increase. Fluent and STAR-CCM+ both captured the initial tank chilldown reasonably well compared to the experiment.

6. References

[1] Moran M, Nyland T and Driscoll S 1991 Hydrogen no-vent fill testing in a 1.2 cubic foot (34 liter) tank NASA TM-105273

[2] Moran M, Nyland T and Papell S 1990 Liquid transfer cryogenic test facility – initial hydrogen and nitrogen no-vent fill data NASA TM-102572

[3] Schrage R 1953 *A Theoretical Study of Interphase Mass Transfer* (New York: Columbia University Press)

Acknowledgments

The authors acknowledge and thank the Cryogenic Fluid Management Modeling Portfolio and Cryogenic Fluid Management Portfolio Project for funding this work. The authors also recognize Matthew Moran for his insight on the experimental setup and data analysis.